

## Modelling the nonlinear behaviour of masonry walls strengthened with textile reinforced mortars

Wang, X.; Ghiassi, Bahman; Oliveira, Daniel V.; Lam, C. C.

**DOI**

[10.1016/j.engstruct.2016.12.029](https://doi.org/10.1016/j.engstruct.2016.12.029)

**Publication date**

2017

**Document Version**

Final published version

**Published in**

Engineering Structures

**Citation (APA)**

Wang, X., Ghiassi, B., Oliveira, D. V., & Lam, C. C. (2017). Modelling the nonlinear behaviour of masonry walls strengthened with textile reinforced mortars. *Engineering Structures*, 134, 11-24.  
<https://doi.org/10.1016/j.engstruct.2016.12.029>

**Important note**

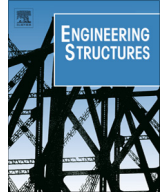
To cite this publication, please use the final published version (if applicable).  
Please check the document version above.

**Copyright**

Other than for strictly personal use, it is not permitted to download, forward or distribute the text or part of it, without the consent of the author(s) and/or copyright holder(s), unless the work is under an open content license such as Creative Commons.

**Takedown policy**

Please contact us and provide details if you believe this document breaches copyrights.  
We will remove access to the work immediately and investigate your claim.



# Modelling the nonlinear behaviour of masonry walls strengthened with textile reinforced mortars



X. Wang<sup>a</sup>, Bahman Ghiassi<sup>b,c,\*</sup>, Daniel V. Oliveira<sup>c</sup>, C.C. Lam<sup>a</sup>

<sup>a</sup> Department of Civil and Environmental Engineering, University of Macau, Macau, China

<sup>b</sup> Department of Civil Engineering and Geosciences, TU Delft, The Netherlands

<sup>c</sup> ISE, University of Minho, Department of Civil Engineering, Azurém, 4800-058 Guimarães, Portugal

## ARTICLE INFO

### Article history:

Received 15 June 2016

Revised 8 November 2016

Accepted 15 December 2016

Available online 27 December 2016

### Keywords:

Historical structures

Strengthening

Textile reinforced mortars (TRMs)

FE simulation

Seismic performance

## ABSTRACT

Textile Reinforced Mortars (TRMs) have found extensive attention for externally bonded reinforcement of masonry and historical structures. However, only few information is available regarding their mechanical properties and effectiveness in improving the seismic performance of strengthened structures. This paper presents an extensive numerical investigation on the effect of TRM composites on the nonlinear response and failure modes of masonry walls. The effect of boundary conditions and the TRM type on the performance of strengthened walls are critically discussed and presented. It is shown that the performance and failure mode of the walls can significantly change after strengthening, an important issue that should be considered at the design stage. Finally, the effect of TRM application on the nonlinear response of a large historical masonry façade in Macau is investigated and presented.

© 2016 Elsevier Ltd. All rights reserved.

## 1. Introduction

Several strengthening techniques have been used and proposed for improving the seismic resistance of masonry structure [1]. Among them, Externally Bonded Reinforcement (EBR) with innovative composite materials has received extensive attention in the last years and has been the subject of several studies. Fibre Reinforced Polymers (FRPs) have been extensively used for this strengthening technique due to their high mechanical strength, low weight and ease of application. These composites, however, show a poor performance in high temperature conditions, are mechanically and thermally incompatible with poor masonry substrates and can affect the hygrothermal performance of the building due to their (relative) impermeability to moisture transfer. The use of new composite materials based on fabrics (or grids) embedded in inorganic matrices has thus recently received attention as a sustainable and a more compatible solution for application to masonry and historical structures [2–6].

These composites are referred with several terms in the literature such as Textile Reinforced Concrete (TRC), Textile Reinforced Mortar (TRM) or Fabric Reinforced Cementitious Matrix (FRCM).

Two key components of TRMs are the matrix and the reinforcing mesh. The most common matrices used for strengthening applications are lime-based or cement-based. The lime-based mortars are proposed for application to masonry and historical buildings due to sustainability and compatibility issues [6]. As for the reinforcement, steel, glass, PBO (polyparaphenylene benzobisoxazole), basalt and natural fibres are among the most common materials employed [6,7]. The variety of available fibres and mortar types lead to a wide range of mechanical properties for TRMs which makes them suitable for fit for purpose design.

The mechanical behaviour of TRMs and their effectiveness in strengthening applications are highly dependent on the mechanical properties of the fibres and the mortar, as well as the bond behaviour at the fibre-to-mortar and mortar-to-substrate interfaces [6,8–10]. Mortars are usually brittle with a relatively low tensile strength (in the order of masonry tensile strength). Fibres have also a linear elastic behaviour until tensile rupture, but with a much larger deformation capacity (generally the tensile rupture strain of the fibres is much larger than mortar cracking strain). Once the mortar is cracked, fibres bridging mechanism (which is dependent on the fibre-to-mortar bond behaviour) becomes activated leading to crack propagation and a pseudo-ductile response of TRM composites [11].

Despite the recent attention on the use of TRMs for strengthening of masonry, the available information regarding the mechanical performance and effectiveness for improving the performance of

\* Corresponding author at: Department of Civil Engineering and Geosciences, TU Delft, 2600 GA, The Netherlands.

E-mail addresses: [allenxuanwang@gmail.com](mailto:allenxuanwang@gmail.com) (X. Wang), [bahmanghiassi@gmail.com](mailto:bahmanghiassi@gmail.com) (B. Ghiassi), [danvco@civil.uminho.pt](mailto:danvco@civil.uminho.pt) (D.V. Oliveira), [fstccl@umac.mo](mailto:fstccl@umac.mo) (C.C. Lam).

masonry structures are still few. Although several recent studies have been devoted to mechanical characterization of TRM composites, fundamental mechanisms that govern the nonlinear response at different levels are still not well studied [12]. At the micro-level, the fibre-to-mortar bond behaviour in different strengthening systems has received few attention, see e.g. [12]. At the component level, mechanical characterization of TRMs has been mostly focused on tensile response, see e.g. [7,12–14], and the available information on flexural and shear response are very limited, see e.g. [15,16]. The bond of TRM-to-masonry has also received extensive attention, see e.g. [6,9,10,12,17–19]. The information regarding the effectiveness of TRMs in improving the seismic performance of masonry structural elements is still very limited, but the number of studies devoted to this subject have been consistently growing during the last years. Investigations at the structural level are mostly focused on the static monotonic (and very few on static cyclic) nonlinear response of strengthened walls under in-plane, see e.g. [2,5,20–27], and out-of-plane actions, see e.g. [26,28,29], as well as nonlinear response of arches, see e.g. [16,30,31].

Application of numerical modelling tools has also been limited and mostly focused on simulation of tensile response, e.g. [32,33], and bond behaviour, e.g. [18,9]. Only few studies can be found in the literature on numerical modelling of TRM-strengthened masonry at the structural level, see e.g. [34–36]. Numerical modelling of TRM-strengthened masonry, although a complex task, is an interesting approach for understanding the influencing parameters on the performance of strengthened structures and the changes of failure modes after strengthening.

Numerical simulations, depending on the desired level of accuracy and on the model size, can be performed following the micro-modelling (usually used for simulating small components) or the macro-modelling approaches (usually used for simulating structural performance) [37,38].

Micro-modelling, in which all the components and the interaction between them are simulated separately, is useful for a detailed analysis and understanding of all possible mechanisms and failure modes. In this technique, all individual components of masonry (unit, mortar and unit-to-mortar interface) and TRM layer (fibre mesh, mortar, fibre-to-mortar interface) are modelled separately. Several material parameters and suitable bond-slip laws for the interfaces are therefore necessary for a reliable simulation. This approach is time consuming (even for small scale models) and requires a fine FE mesh size to resolve the mesh dependency of the interface elements, and the analysis is computationally demanding and expensive.

On the other hand, in macro-modelling masonry and TRM are simulated as continuum elements with the nonlinearities homogenized over the elements. The average response of masonry and TRM are therefore considered in the phenomenological constitutive laws. This technique, which requires knowledge on the macro properties of each composite, is usually used for structural level investigations. The use of macro-models for structural level simulations is still at early stage for TRM-strengthened masonry, average constitutive models are not available, and the appropriateness of the existing damage/crack models is not clear yet. These two later issues require further comprehensive experimental tests on the nonlinear shear and flexural response of TRMs.

This paper presents a numerical investigation on the in-plane behaviour of TRM-strengthened masonry panels following the macro-modelling approach. The main objective is to investigate the effectiveness of different, commercially available, TRM composites on the nonlinear behaviour and failure mode of masonry walls. The nonlinear behaviour of masonry and TRM are represented by a macroscopic smeared crack approach with the assumption of perfect bond between masonry and TRM layers.

Although the inclusion of interface elements between TRM and masonry is an easy task and can be considered in the same framework, the assumption of perfect bond is reasonable (and has also been made by other authors) as (i) experimental results have shown this failure is unlikely to occur, see e.g. [34] and (ii) occurrence of such a failure should be avoided at the design stage by selecting a suitable mortar type (through bond tests) to ensure the effectiveness of this strengthening system. The masonry is modelled assuming a softening anisotropic elasto-plastic continuum model [39] following the rotating smeared crack approach. The TRM layer is modelled by assuming an isotropic behaviour for the mortar (with a parabolic behaviour in compression and a tension softening law) with embedded reinforcements perfectly bonded to the mortar. This latter assumption is also reasonable as (i) the experimental results have shown that slippage of the fibres from the mortar can be avoided if the bond length is sufficiently long and (ii) even if slippage occurs, its effects can be considered in the model by modification of the mortar tension softening law and fibres' stiffness.

The accuracy of the modelling strategy is initially validated at the component level by comparing the numerical results with some experimental data taken from the literature. The model is then used for simulating the nonlinear response of TRM-strengthened masonry panels by performing static nonlinear (pushover) analysis. Finally, the effect of TRM application (considering different TRM types and strengthening schemes) on the nonlinear response of real a historical masonry façade in Macau is investigated and presented.

## 2. Modelling of TRM composites

This section discusses the adopted numerical modelling technique and its validation for simulating the nonlinear behaviour of TRM composites. Validation is performed by comparison of numerical results with experimental tests taken from literature. Due to the lack of available experimental data on the shear response of TRM panels, tensile tests performed by Carozzi and Poggi [14] are selected as reference. The main focus is on validation of the modelling strategy and constitutive models with particular attention to the FE mesh size and mortar tension softening law.

The total strain rotating crack model is adopted for modelling the nonlinear response of the mortar. Rotating smeared crack models seem suitable for simulating the nonlinear response of TRMs and have been used elsewhere, see e.g. [34,36]. Further comprehensive experimental tests on the TRMs behaviour under in-plane shear and out-of-plane loading conditions are however necessary for an in-depth understanding of suitable modelling approaches and development of better constitutive and damage models for these materials.

### 2.1. Reference experimental results

The tensile tests performed by Carozzi and Poggi [14] on TRM composites made of cementitious mortar and PBO (polypara-phenylene benzobisoxazole) fibre grids are selected as reference. The PBO fibres were organized in an unbalanced net made of 10 mm and 20 mm spaced rovings in longitudinal and transverse directions, respectively (Fig. 1a). The grid had an equivalent thickness of 0.046 mm and 0.011 mm in longitudinal and transverse directions, respectively. The materials mechanical properties, presented in Table 1, were obtained by performing tensile tests on single dry rovings and fibre grid strips (made of four rovings), and compressive and indirect tensile tests on mortar specimens (Table 1). Further details about the test methods and procedures can be found in [14].

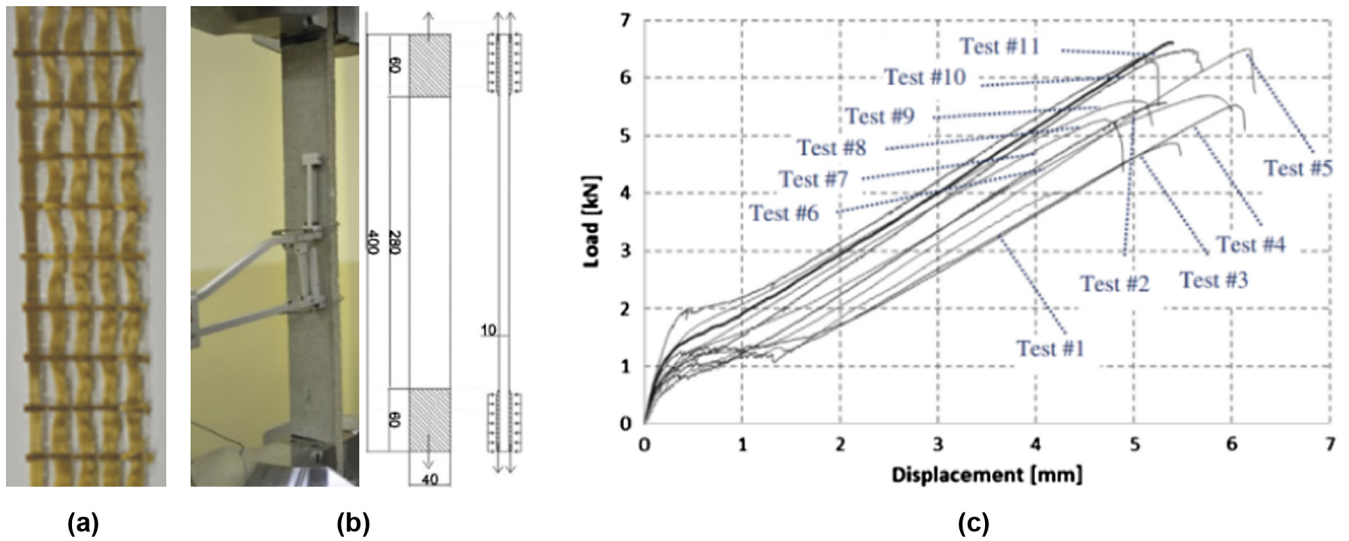


Fig. 1. Reference experimental tests: (a) PBO grid; (b) tensile test set-up (dimensions in mm); (c) experimental load–displacement curves, taken from [14].

**Table 1**  
Mechanical properties of PBO fibres and cementitious mortar in the tests [14] and in the FE model.

Material	Test specimen	# test	Failure stress (MPa)	C.o.V (%)	E (GPa)	C.o.V (%)
PBO	Single roving	6	3905	3.2	216	20.8
	Fibre grid <sup>a</sup>	4	3397	7.2	–	–
	FE model adopted	–	3400	–	188	–
Mortar	Tensile test (Brazilian)	7	4.75	4.05	>6 (data sheet)	–
	Compressive test	–	15 (data sheet)	–	–	–
	FE model adopted	–	3.56 (tensile) 15 (compressive)	–	4.2	–

<sup>a</sup> 4 cm width with 4 rovings, roving in the warp direction.

The tensile tests were performed on TRM coupons with nominal size of  $400 \times 40 \times 10 \text{ mm}^3$  (Fig. 1b) by direct application of the clamps on the mortar at both ends. High compressive stresses were applied to the mortar by the clamping system to avoid slipping of the fibres [14]. A significant variability in the transversal section of the specimens (both width and thickness) was observed which led to quite a wide experimental scatter in the load–displacement curves (Fig. 1c). The typical tri-linear tensile behaviour associated to TRM composites was observed in all the specimens: (I) the un-cracked stage, in which the mortar matrix contributes to both load bearing capacity and stiffness; (II) the crack development stage, during which crack pattern develops progressively; (III) cracked stage, in which the crack pattern has completely developed and the response is governed by the tensile behaviour of fibres.

## 2.2. Finite element model

The modelling and analysis were performed using the commercial FE package DIANA 10 [40]. A macro-modelling approach based on smeared crack theory, with the assumption of having a homogenized layer of mortar with distributed reinforcements, is followed. The adopted mesh included quadrilateral 8-noded curved shell elements (denoted as CQ40S in DIANA) for the mortar matrix and embedded reinforcements for the fibre grids, see Fig. 2. The reinforcement grids are modelled as fully embedded in the mortar matrix elements (using grid elements in DIANA FE package) and therefore their displacements and strains are fully coupled with the host elements (mortar in this case). The reinforcements therefore do not have degrees of freedom of their own and their strains

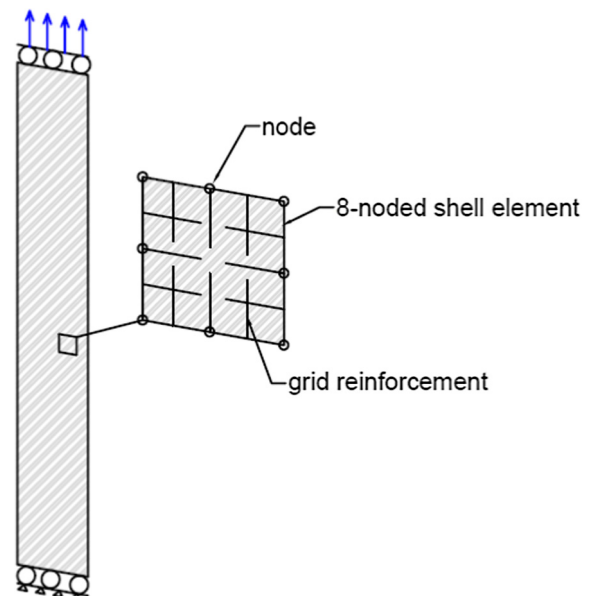


Fig. 2. Adopted FE mesh, boundary condition and loading scheme.

are computed from the displacement field of the mortar matrix elements which implies perfect bond between the reinforcement and the surrounding material. It should be noted that the DIANA package allows to consider bond-slip laws for the embedded reinforcements. However, such a modelling requires individually

simulation of each fibre and therefore is not suitable for large structural simulations.

The constraints and loading conditions were applied to the model according to the experimental test setup and conditions.

### 2.3. Material properties, boundary condition and analysis procedure

The boundary conditions and loading scheme were set according to the tests, see Fig. 2. The specimen's self-weight was not included in the model as it was insignificant when compared to the applied load. The nodes at the bottom and top of the model were fixed in the vertical and horizontal directions to simulate the experimental conditions. A static nonlinear analysis was performed by application of an incremental vertical displacement (displacement control analysis) at the top nodes, see Fig. 2. The modified Newton-Raphson iterative scheme together with the line search method and an energy convergence criteria (with an acceptance tolerance of 0.0001) were used for solving the nonlinear equations.

The total strain rotating crack model is adopted for modelling the nonlinear response of the mortar. Two softening models, including a typical exponential softening model (Fig. 3a) and the JSCE [41] softening model (Fig. 3b), are used for cracked mortar to investigate the effects on the nonlinear response. A parabolic compression model is used (Fig. 3c) for simulating the mortar behaviour under compressive stresses. The main mechanical properties were derived from the experimental results (Table 1). For the tensile strength of mortar,  $f_t$ , and elastic modulus  $E$ , a factor of 0.7 was applied to the results obtained from the Brazilian tests [42] to convert these results to direct tensile properties. The ultimate tensile strain,  $\epsilon_{tu}$ , was given 0.00224. According to the experimental results, a linear elastic behaviour until failure with an elastic modulus,  $E$ , of 188 GPa and tensile strength,  $f_t$ , of 3400 MPa was used for the PBO-grid.

## 2.4. Results and discussion

### 2.4.1. Effect of FE mesh size

The dependency of the numerical results on the FE mesh size was initially investigated and the results are presented in this section. Different models with mesh element sizes of 2.5, 5, 10, and 20 mm were produced and analysed. The exponential tension softening model for mortar is used in this section. The numerical load-displacement curves (applied load vs. displacement in vertical direction at top of the specimen, see Fig. 2) are presented in Fig. 4 in comparison with the envelope of the experimental results. It can be observed that all mesh sizes exhibit a clear tri-linear behaviour, as expected. The failure displacement and corresponding maximum loads are similar in all the models, and only a slight difference can be observed in the second phase (crack development

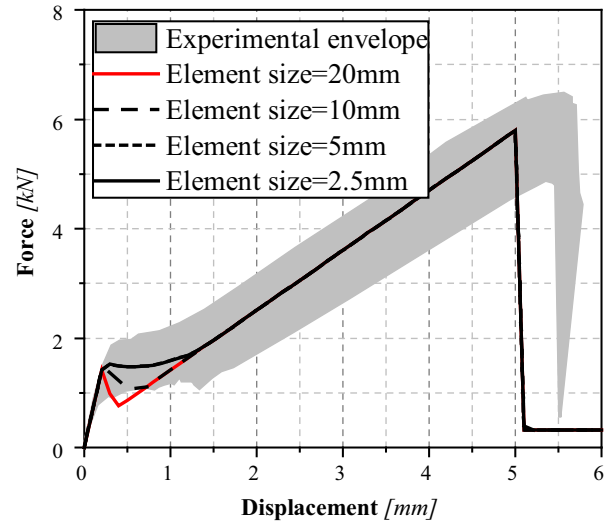


Fig. 4. Influence of mesh size on the tensile response.

phase). The results converge in the specimens with FE mesh size of  $l \leq 5$  mm (corresponding to 448 elements in the model) and therefore this size was selected for simulations in the next sections.

### 2.4.2. Effect of tension softening model

There is still a lack of information on suitable constitutive models for simulating the nonlinear response of TRM composites. The large variety of mortars and fibres used in real applications have made the characterization and constitutive modelling challenging. The effect of tension softening law, as one of the main numerical inputs in smeared crack modelling approaches, on the nonlinear response of TRMs is investigated in this section. Two different constitutive models are used (Fig. 3a and b): (1) exponential tension softening and (2) JSCE [41] tension softening model. The exponential softening model is one of the most common constitutive laws used for representing the softening behaviour of concrete and mortar after cracking. On the other hand, it seems that a plateau after cracking, and before the tension softening part, can appropriately simulate the tensile response of TRMs in the crack development and stabilization phase. JSCE model [41] consists of a plateau after cracking, which is followed by tension softening according to the following formula:

$$\sigma = f_t (\epsilon_{tu} / \epsilon)^c \quad (1)$$

where  $\sigma$  is the tensile stress,  $\epsilon$  is the total tensile strain,  $f_t$  is the tensile strength,  $\epsilon_{tu}$  is the tensile strain corresponding to the end of plateau and  $c$  is the power parameter usually taken as 0.4 for unreinforced concrete and as 0.2 for reinforced concrete elements.

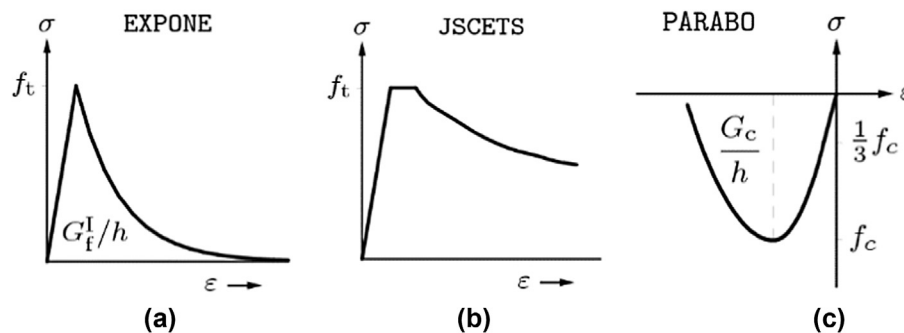


Fig. 3. Constitutive models used for mortar: (a) exponential tension softening model (b) JSCE tension softening model (c) parabolic compression model.

The numerical load–displacement curves are presented in comparison with the envelope of the experimental results in Fig. 5. The numerical results show a good agreement with experimental data for both tension softening models, not only in terms of the peak load and ultimate displacement but also the stiffness and post-cracking behaviour. The numerical curves generally fall within the experimental envelope and show the typical trilinear behaviour of TRMs under tensile loading.

Fig. 5b shows the existence of the plateau in the JSCE model leads to a smoother transition zone in the numerical results. However, the resisting forces in the second and third stages are slightly larger than in the exponential model (although still inside the experimental envelope). This can be due to the existence of the plateau or the value chosen for the parameter  $c$ , both directly related to the tensile fracture energy. The latter is investigated in Fig. 5c–d through a parameter study on the effect of  $c$  value on the tensile response of TRMs. The load–displacement curves, see Fig. 5d, show that numerical results are closest to the average experimental results when  $c = 0.4$ – $0.8$ . It should be noted that  $c = 0.2$ , usually used for RC elements, does not lead to a suitable tensile response due to the large residual tensile stresses and fracture energy. The bond mechanism between the reinforcement and mortar is different in TRMs than RC elements due to both mortar and reinforcement properties and thus a different  $c$  value should be used in these elements. It should be noted that the observed results are also affected by the mortar tensile strength which has been assumed as 75% of the tensile strength obtained from the Brazilian tests.

In conclusion, both tension softening models provide sufficiently accurate numerical results in terms of global load–displacement curves. It seems, however, that the JSCE model leads

to a clearer and more realistic transition zone in the second stage and has a better physical compatibility with the nonlinear phenomenon, and it is thus used hereafter (with  $c = 0.4$ ).

### 3. In-plane behaviour of strengthened masonry panels

The main objective of this section is to investigate the changes in the nonlinear response and failure mode of brick masonry panels after strengthening with different TRM composites, an important issue that has not yet received attention in the literature.

A panel with dimensions of  $1000 \times 1000 \times 100 \text{ mm}^3$  (height  $\times$  width  $\times$  thickness) is considered, see Fig. 6. The nonlinear response of the panel, under vertical pre-compression and lateral loads is initially investigated by performing static nonlinear (pushover) analysis. The masonry panel is then strengthened, on both faces, with different TRM composites (different reinforcement materials, same mortar properties and TRM total thickness of 5 mm). The effect of strengthening on the nonlinear response and failure mode of the panels is investigated and discussed next. The TRM thickness has been chosen 5 mm as: (i) the overall thickness of TRM systems is usually in the range of 5–10 mm (ii) several experimental studies have shown that the effect of mortar thickness is negligible in this range of variations and (iii) several experimental results available in the literature have been followed considering a 5 mm thickness [6,12].

The detailed list of selected panels and strengthening materials/details is presented in Table 2. Three different pre-compression levels of 0.00 MPa (REF1, no vertical stress), 0.85 MPa (REF2, moderate vertical stress) and 2.55 MPa (REF3, high vertical stress), corresponding to 0%, 10% and 30% of the compressive strength, are considered. One of the panels, REF4, is modelled without any

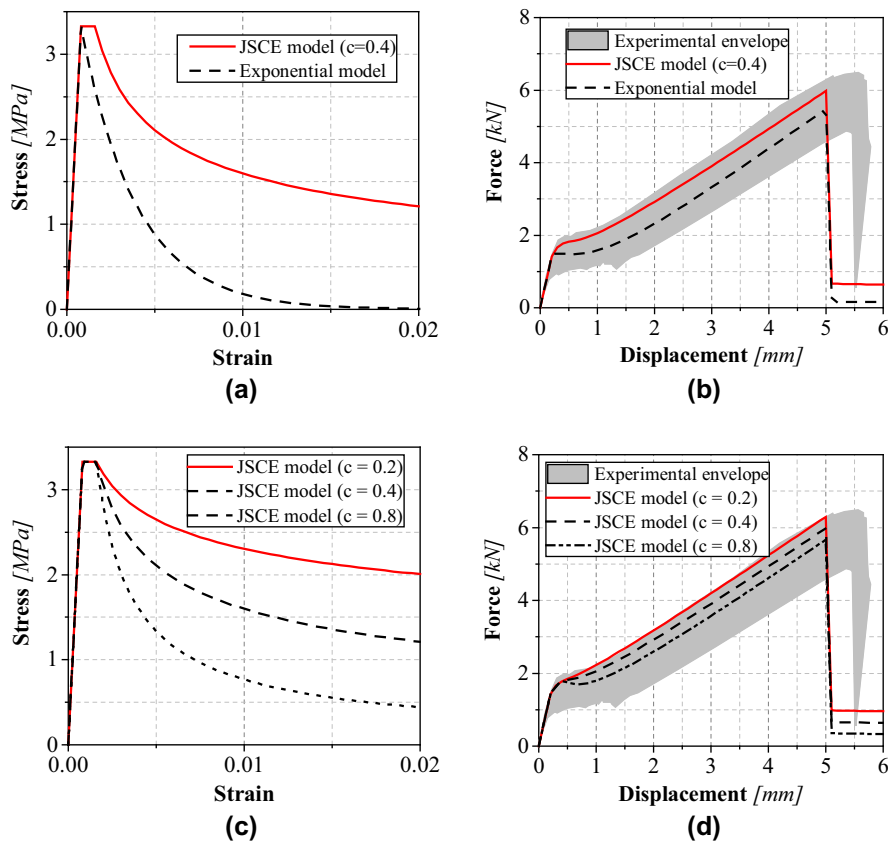


Fig. 5. Comparison of numerical and experimental results: (a) exponential and JSCE softening models; (b) load–displacement curves; (c) JSCE softening models with different parameter  $c$ ; (d) effect of JSCE's parameter  $c$  on the load–displacement curves.

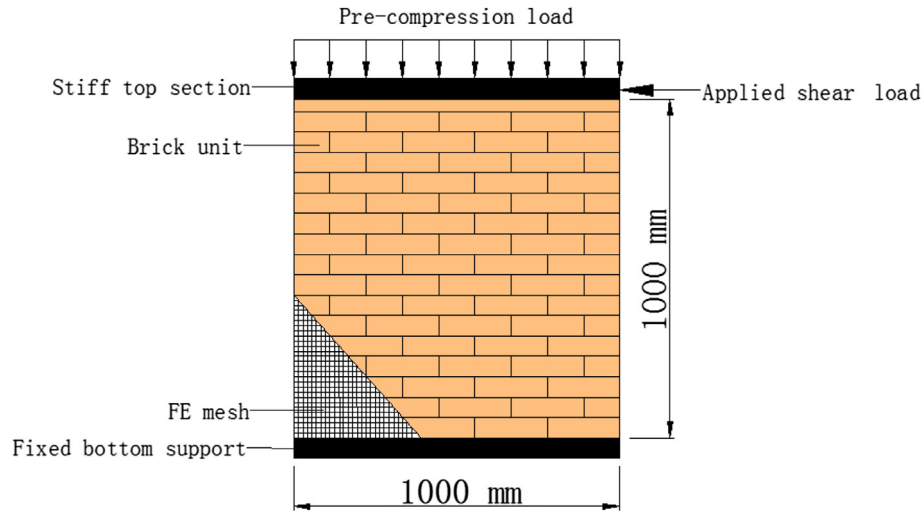


Fig. 6. Geometry and loading condition of the panel.

**Table 2**  
Hypothetical panels considered for the analysis.

Analysis	Boundary condition at top	Pre-compression stress (MPa)	Reinforcement type
REF1	Free	0.00	No strengthening
REF2	Free	0.85	No strengthening
REF3	Free	2.55	No strengthening
REF4	Closed	0.00	No strengthening
REF2-1	Free	0.85	Steel
REF2-2	Free	0.85	PBO
REF2-3	Free	0.85	Basalt
REF2-4	Free	0.85	Glass
REF3-1	Free	2.55	Steel
REF3-2	Free	2.55	PBO
REF3-3	Free	2.55	Basalt
REF3-4	Free	2.55	Glass
REF4-1	Closed	0.00	Steel
REF4-2	Closed	0.00	PBO
REF4-3	Closed	0.00	Basalt
REF4-4	Closed	0.00	Glass

pre-compression level but constrained against vertical displacements at top. This analysis is aimed at stimulating the pure shear response of strengthened panels and therefore is useful for understanding the nonlinear shear response. Moreover, such boundary conditions can occur in infill frames in which the panel can be subjected to shear stresses without allowance of vertical deformation. It should also be noted that although no direct pre-compression load is applied to the panel, vertical load is automatically introduced in the panels because the vertical displacements are constrained.

Panels REF2, REF3 and REF4 are strengthened with four different TRMs, as presented in Table 2, leading to a total of 16 panels. The reinforcing materials consist of the most conventional types used for strengthening projects and include PBO, steel, glass and basalt fibres.

### 3.1. Finite element model

A two-dimensional nonlinear Finite Element (FE) model was prepared in FE package DIANA 10 [40] for simulating the nonlinear response of URM and strengthened panels. Both masonry and TRM layers are modelled following a macro-modelling strategy. Each are made of a single shell layer consisting of eight-node shell ele-

ments (denoted by CQ40S in DIANA) with an element mesh size of 5 mm. The strengthened panels are made of two shell layers (URM and TRM) perfectly bonded together. The assumption of perfect bond between masonry and TRM is reasonable and has already been discussed in Section 1, see also [34,36].

The masonry is modelled assuming a softening anisotropic elasto-plastic continuum model [39] following the rotating smeared crack approach. The model consists of a Hill-type yield criterion in compression and a Rankine-type yield criterion in tension. This material model is well known for simulating the nonlinear response of masonry panels and has been widely used and reported in the literature, see e.g. [43–45]. The mechanical parameters of the brick masonry, presented in Table 3, are selected based on numerical data from Grande et al. [44] and modified according to the experimental data from material characterization tests. The material characterization tests were performed at University of Macau on solid clay grey brick which is a key material in Chinese traditional architecture [46].

The TRM layer is modelled assuming an isotropic continuum model following the rotating smeared crack approach for the mortar. A parabolic model in compression and the JSCE tension softening model in tension (with  $c = 0.4$ ) are used. The mortar properties

**Table 3**  
Mechanical parameters of masonry.

Masonry mechanical parameters		
Young's Modulus (MPa)	( $E$ )	8000
Poisson's ratio	( $\nu$ )	0.15
Tensile strength along $x$ -direction (MPa)	( $\sigma_{tx}$ )	0.25
Tensile strength along $y$ -direction (MPa)	( $\sigma_{ty}$ )	0.35
Compressive strength along $x$ -direction (MPa)	( $\sigma_{cx}$ )	7.80
Compressive strength along $y$ -direction (MPa)	( $\sigma_{cy}$ )	8.50
Fracture energy in tension along $x$ -direction (N mm/mm <sup>2</sup> )	( $G_{fx}$ )	0.018
Fracture energy in tension along $y$ -direction	( $G_{fy}$ )	0.054
Fracture energy in compression along $x$ -direction (N mm/mm <sup>2</sup> )	( $G_{fcx}$ )	15.00
Fracture energy in compression along $y$ -direction (N mm/mm <sup>2</sup> )	( $G_{fcy}$ )	20.00
Factor that determines the shear stress contribution to the tensile failure	( $\alpha$ )	1.0
Factor which couples the normal compressive stress	( $\beta$ )	-1.0
Factor which controls shear stress contribution to compressive failure	( $\gamma$ )	3.0
Factor that specifies the equivalent plastic strain corresponding to the peak compressive stress	( $k_p$ )	0.0012

\* Here  $x$  is the head joint direction and  $y$  is the bed joint direction.

**Table 4**  
Mechanical parameters of reinforcement materials considered for analysis.

Material	$E$ (GPa)	$f_t$ (MPa)	Spacing (mm)	Cross section (mm <sup>2</sup> )	Reinforcement ratio (mm <sup>2</sup> /m)	Geometry	Density (g/m <sup>3</sup> )
PBO	188	3400	10.00	0.410	41.0	UBG, SM	–
Steel	206	3200	6.37	0.538	84.5	BG, SM	670
Glass	72	1290	25.00	0.850	34.0	BG, SM	225
Basalt	89	1542	6.00	0.230	38.3	BG, SM	250

Where: UBG = unbalanced grid, BG = balanced grid, SM = squared mesh.

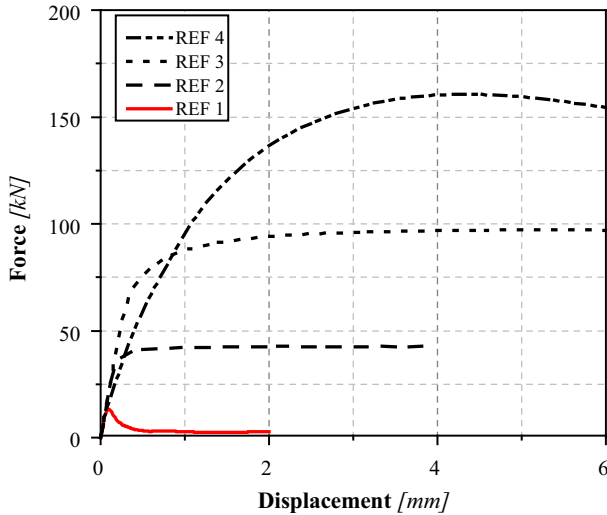


Fig. 7. Numerical load–displacement curves of URM panels.

are chosen the same as used in the last section. The reinforcements are assumed embedded in the mortar with an elastic behaviour until failure and perfect bond with the mortar. The mechanical and geometrical properties of the reinforcing meshes are selected based on the technical datasheets of available commercial products in the market and are presented in Table 4.

The panels are assumed fixed at the bottom and clamped at top with a stiff steel beam with rotational constrains. The pre-compression loading is initially applied, then an incremental horizontal displacement is applied at top (in the middle height of the steel plate) as shown in Fig. 6. The modified Newton-Raphson iterative scheme together with the line search method is used for solving the nonlinear equations.

It should be noted that the numerical results are usually subjected to errors associated with the assumptions and limitations of the simulation technique and materials' constitutive models. TRMs present complex and in some cases unknown failure modes that should be taken into account in the adopted modelling strategy [37,47]. The most important failure modes are matrix-cracking, debonding of the fibre from the matrix, tensile rupture of the fibres [47], and splitting of the mortar. The matrix-cracking and tensile rupture of the fibres are accounted in the simulation through the adopted material models. The effect of fibres-to-mortar bond beha-

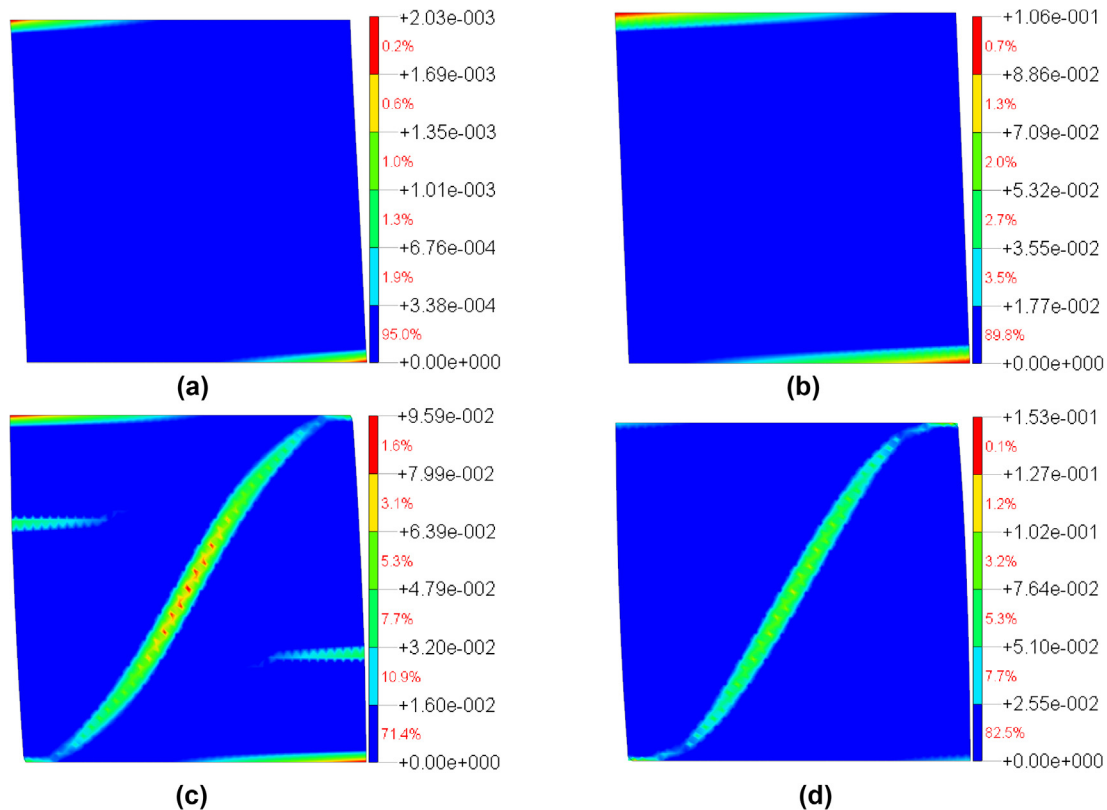


Fig. 8. Equivalent plastic tensile strains at peak load in URM panels: (a) REF1; (b) REF2; (c) REF3; (d) REF4.

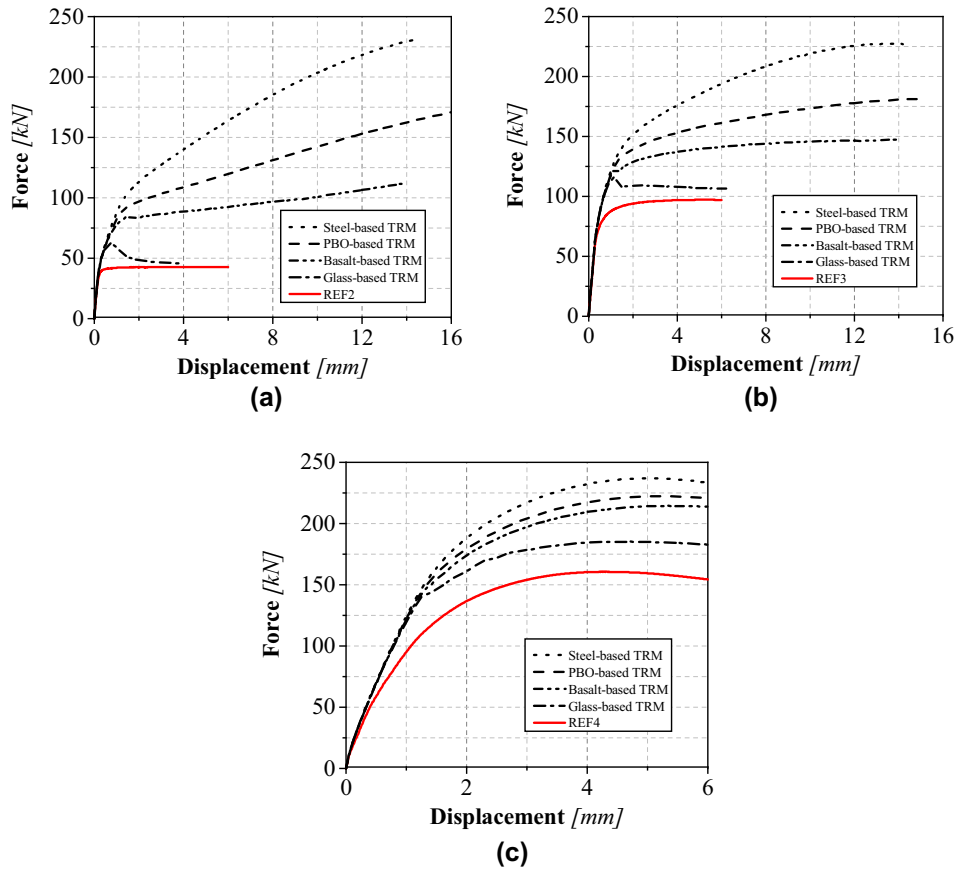


Fig. 9. Numerical load–displacement curves of strengthened panels: (a) REF2; (b) REF3; (c) REF4.

viour at the structural level can be considered by assuming an appropriate tension softening behaviour for the mortar. The exponential tension softening model, presented and validated in the last sections, is adopted in this study to account for this phenomenon. The splitting of the mortar can be simulated through specific damage models or by simply application of a reduction factor to the mortar tensile strength. This has not been considered

here and should be further investigated in future studies. Fibres slipping at the edges or at the connections with other elements, if not avoided, should also be considered in the numerical simulations. This failure can be indirectly considered by application of reduction factors on the tensile strength and stiffness of the fibres or by directly modelling the fibres slippage with the aim of interface elements. Some FE packages, such as DIANA, offer the possibil-

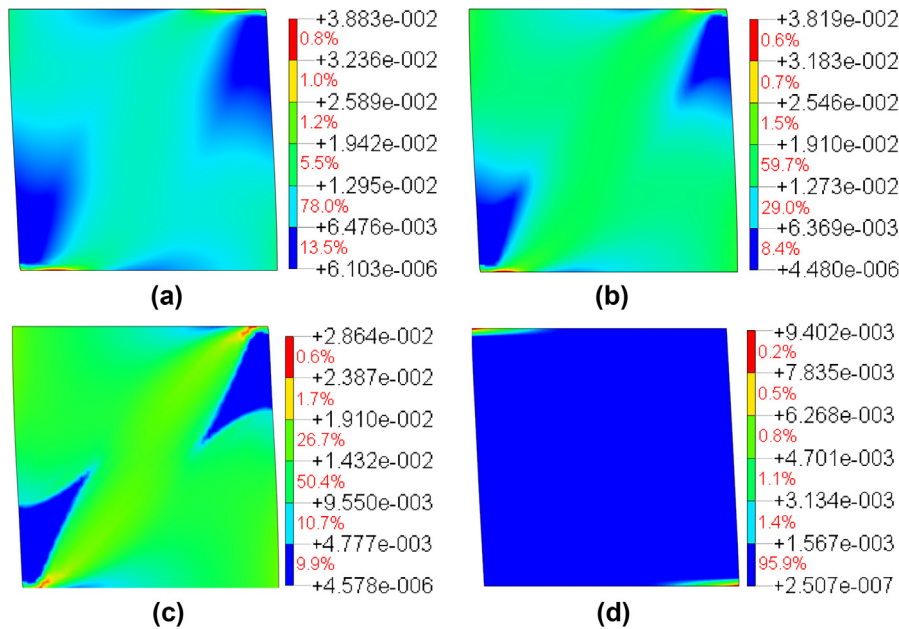


Fig. 10. Principal tensile strains at peak load in TRM-strengthened REF2 panels: (a) steel-based TRM; (b) PBO-based TRM; (c) basalt-based TRM; (d) glass-TRM strengthening.

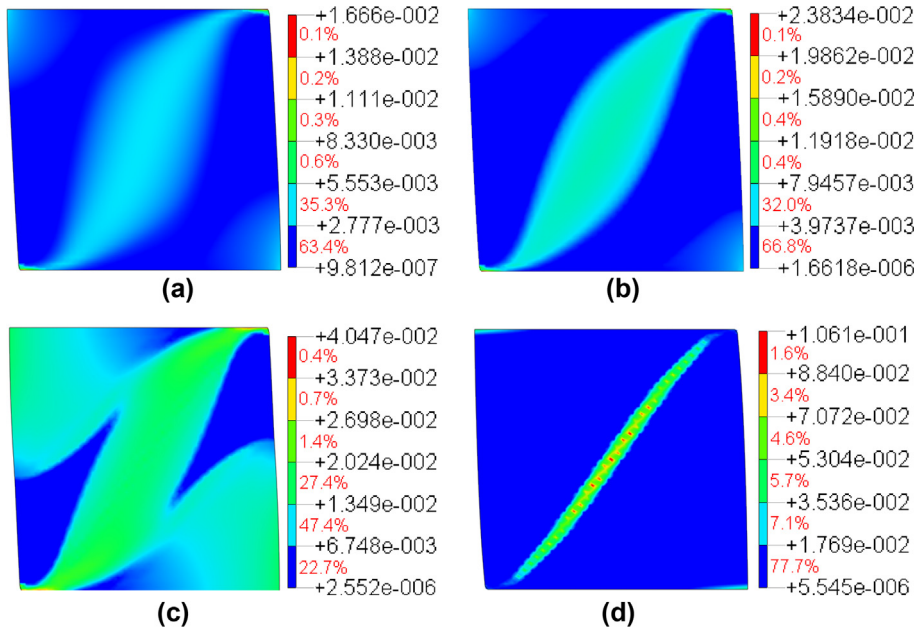


Fig. 11. Principal tensile strains at peak load in TRM-strengthened REF4 panels: (a) steel-based TRM; (b) PBO-based TRM; (c) basalt-based TRM; (d) glass-TRM strengthening.

ity of assuming a bond-slip law for the embedded reinforcements. In this case, however, the reinforcements should be modelled individually making the modelling process extremely time consuming

even for small models. Here it is assumed that the reinforcements are applied with connectors or are wrapped to the walls and therefore no slippage occurs at the wall edges.

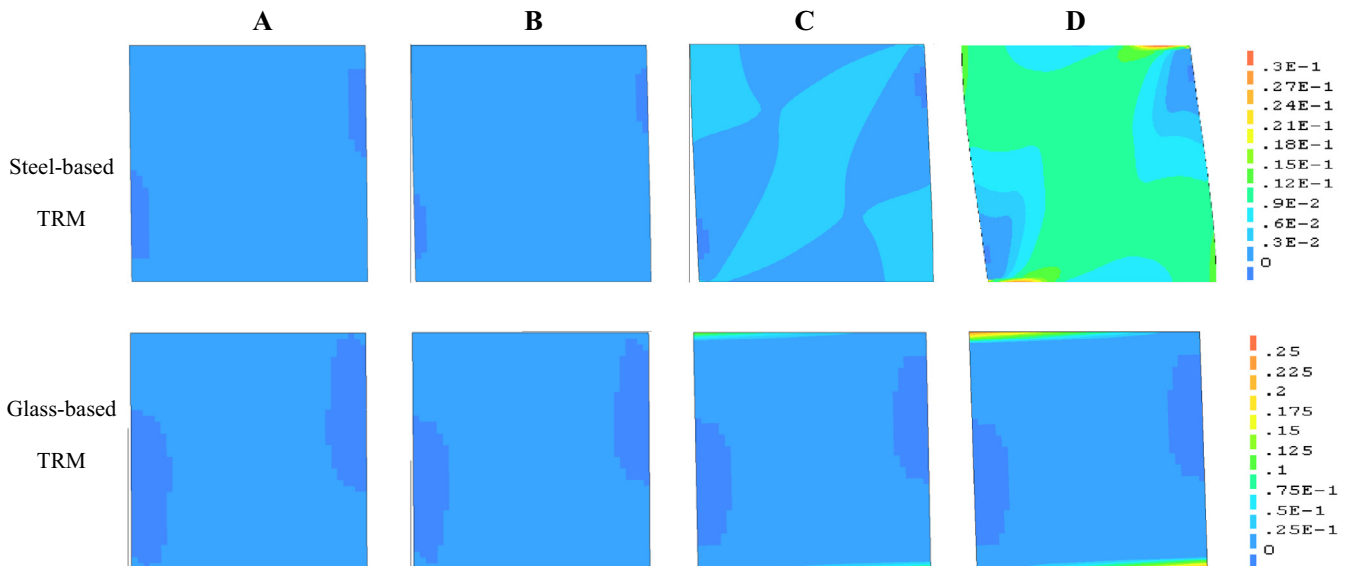
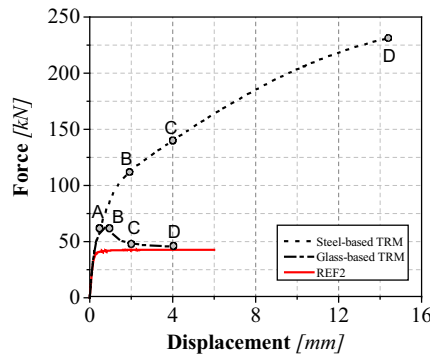


Fig. 12. Principal plastic strains in REF2 strengthened panels.

### 3.2. Results and discussion

#### 3.2.1. URM panels

The numerical load-displacement curves of the URM panels are shown in Fig. 7. It can be observed that the peak load increases significantly with increment of the pre-compression level. While the panel with no pre-compression, REF1, has a lateral load resistance of 13 kN, panels with 0.85 and 2.55 MPa pre-compression levels (REF2 and REF3) exhibit a lateral load resistance of 42 kN and 95 kN, respectively. As expected, panel REF4 shows the maximum load resistance (160 kN) due to its specific boundary condition. The contour of equivalent plastic strains at the peak load are presented in Fig. 8. The formation of plastic strains and the deformation of the panels REF1 and REF2 resembles a rocking failure mode. This failure mode was expected due to the low compressive stresses applied to the panels in these cases. On the other hand, the plastic strains have formed a diagonal strip in REF3 and REF4 panels due to the high compressive stresses and boundary conditions in these panels. This configuration shows that a diagonal tensile cracking has occurred in these two panels.

#### 3.2.2. Strengthened panels

The numerical load-displacement curves for TRM-strengthened panels and the contour of principal tensile strains at the peak load for each panel and strengthening material are shown in Figs. 9–11. The results clearly show the effect of different TRM composites on the nonlinear response and failure mode of the strengthened panels. The last shown point in the numerical curves corresponds to the tensile failure of the fibres, after which, the strengthening system and consequently the masonry wall fail.

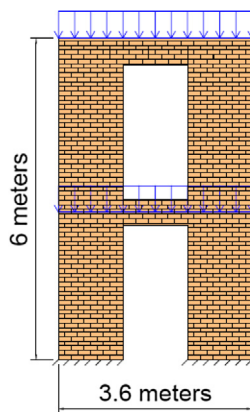


Fig. 13. Geometry, boundary condition and loading.

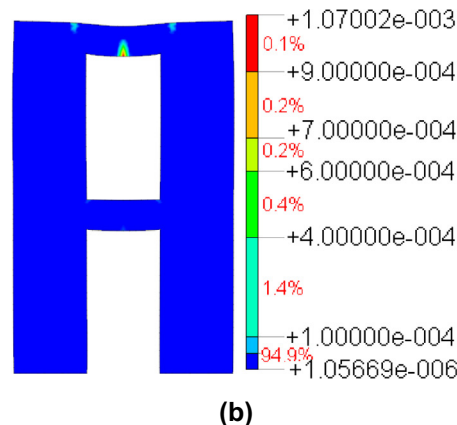
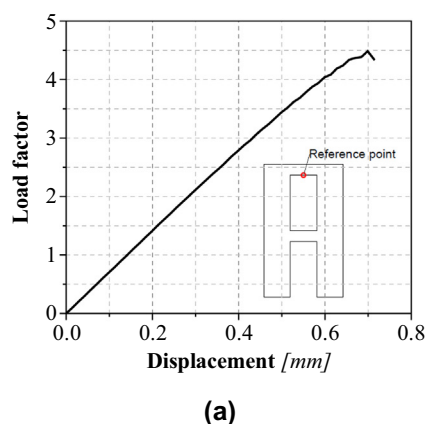


Fig. 14. FE result of single URM façade for overload analysis: (a) capacity curve; (b) principal tensile strain at maximum load factor.

It can be observed that, in all cases, the steel-based TRM strengthened panels show the highest capacity and ductility, followed by PBO-, basalt-, and glass-based strengthened systems. This was expected as the reinforcement ratio and stiffness of the strengthening systems used in this study follow the same trend, see Table 4. No specific difference can be observed in the linear elastic range response of the panels strengthened with different TRM composites. This was expected as the behaviour in this range is controlled by the elastic stiffness of the masonry panel and the mortar layer. After cracking, however, the curves follow different trends depending on the reinforcement ration and stiffness of the reinforcement.

In TRM-strengthened REF2 panels, the failure mode of the panels strengthened with steel, PBO and basalt fibres is distributed diagonal tensile cracking, Fig. 10a–c. These panels therefore show a change of failure mode after strengthening (rocking failure occurred in URM REF2 panel, Fig. 8a). On the other hand, the failure in the panel strengthened with glass-based TRM is rocking at the base, Fig. 10d (similar to the URM panel). For a clearer presentation of the evolution of different failure modes, the distribution of plastic strains on the steel-based and glass-based strengthened panels is presented at different stages of load-displacement curve Fig. 12. The development of diagonal tensile cracks and rocking failure mode in steel-based and glass-based strengthened systems, respectively, can be observed. The difference in the failure modes is also obvious in the force-displacement curves. It can be observed that the glass-based strengthened panel shows a gradual decrement of the load resistance after mortar cracking until reaching the load-displacement curve of the URM panel. On the other hand, the lateral resistance increases with lateral displacements in steel-based TRM system until occurrence of the fibres' tensile rupture.

TRM-strengthened REF3 panels show a similar failure mode as TRM-strengthened REF2 panels and therefore the principal tensile strains are not presented separately. In this case, however, the strengthened panels with steel-, PBO-, and basalt-based TRM composites show a similar failure mode as the URM REF3 panel, Fig. 8b.

The specific boundary conditions assumed for REF4 panels have led to diagonal tension cracking failure mode even in all URM and strengthened panels, Fig. 11. The increase in the load resistance of this panel after strengthening is less than the other two panels (REF2 and REF3). Here, it seems that the strengthened panels have larger elastic stiffness in comparison to the URM panel.

## 4. The case study: Patio da Felicidade façade in Macau

Most of the existing historical structures in Macau are made of stone or clay brick masonry. Some of these existing unreinforced

masonry structures need efficient retrofitting as they are suffering deterioration or damage due to environmental conditions or mechanical loads. This section is devoted to evaluation of the seismic performance and strengthening of a masonry façade in the historic centre of Macau. The detailed discussion of the selected case study together with the analysis details and results are given next.

4.1. Description of the case study

The “Historic Centre of Macau” is the oldest and the most complete and consolidated array of European architectural legacy standing intact on Chinese territory. This historic centre is located on the west of Avenida Almeida Ribeiro, the most famous business street in Macau. Rua da Felicidade, located in this centre, was known as the red light district of Macau from 1920 s to 1960 s. Patio da Felicidade, located in the back line of Rua da Felicidade, is built of clay brick with mortar joints in the late 19th century and represents a typical Lingnan style of architecture for shop houses in south China. A typical façade in the Patio da Felicidade is selected here as the case study. The façade consists of nine shop houses connected together along the street.

The analysis is performed at two stages. In the first stage, the performance of a single two-story shop house (denoted as single façade throughout the paper) is investigated. In the second stage, the whole façade is simulated and investigated. The single façade has 3.6 m length, 6 m height and 0.2 m thickness. The dead load from the floors (roof and first floor) was applied on the façade, according to the real conditions, as a distributed load with 5 kN/m (for the roof) and 2 kN/m (for the first floor), respectively.

4.2. Behaviour of the single façade

The geometry, boundary condition and applied dead loads at the roof levels are shown in Fig. 13. The façade is considered fixed at the bottom. The masonry is modelled with the same material properties as presented in Table 3 and following the same modelling strategy as presented in Section 3 (8-node curved shell CQ40S elements with a softening anisotropic elasto-plastic continuum material model).

A nonlinear static analysis (pushover) is performed initially on the structure under its self-weight to obtain its safety factor against vertical loads. Then a lateral pushover analysis, in combination with the structure’s self-weight, is performed on the structure. The lateral loads are applied based on the mass distribution along the structure.

4.2.1. Nonlinear behaviour of URM façade

4.2.1.1. Self-weight analysis. The capacity curve of the structure under self-weight pushover analysis and the principal tensile strains at the maximum load factor are presented in Fig. 14. The safety factor of the façade under its self-weight is estimated as 4.49 being a relatively high value. The principal tensile strains show that the cracks mainly occur at the middle and corners of the top spandrel due to the larger distributed dead loads at this level in comparison to the first floor.

4.2.1.2. Pushover analysis. The pushover analysis is performed based on application of incremental horizontal forces proportional to the mass of the structure. The vertical loads from the roof weight

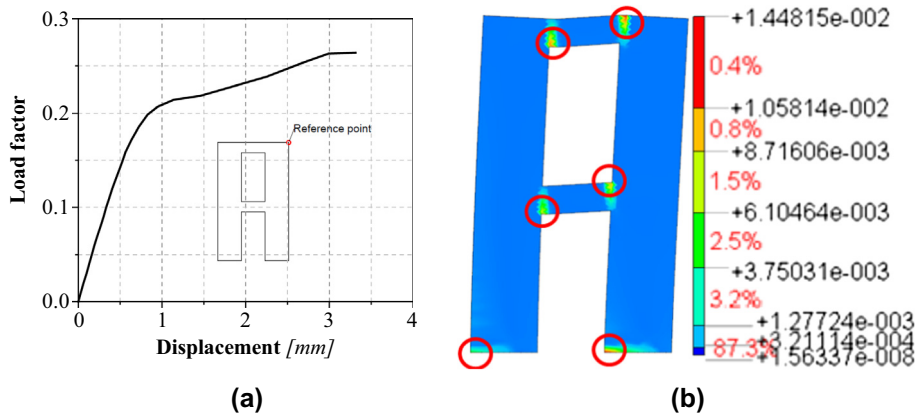


Fig. 15. Pushover analysis results: (a) load–displacement curve of single URM façade; (b) principal tensile strain contour at peak load.

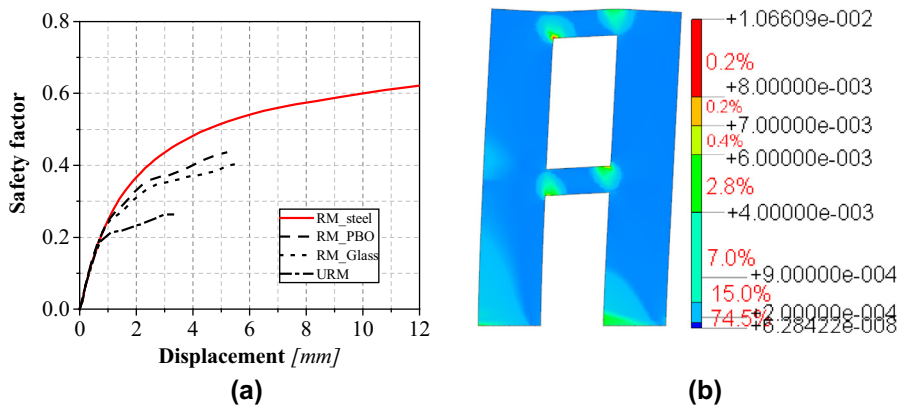


Fig. 16. Pushover analysis results: (a) load–displacement curve of single strengthened façade; (b) principal tensile strain contour for RM\_steel at peak load.

and the first floor slab were also taken into account to the seismic mass of the structure. The capacity curve of the URM façade under lateral loads is presented in Fig. 15a. The control node for the horizontal displacement is chosen at the right top corner, as shown in the figure. The nonlinear behaviour of the structure starts at a very early stage (around 0.5 mm lateral displacement) and the load factor,  $\alpha$ , reaches the maximum value of 0.26 at the last point. This load factor is quite low, although it should be noted that in reality the façade is connected with the surrounded buildings composing a long façade.

Fig. 15b shows the principal tensile strains at the peak load ( $\alpha = 0.26$  and displacement = 3.31 mm) for the URM façade. The main cracks and failure points are marked with red circles in this figure. The largest cracks are located at the corner of openings and at the base of the façade, as expected. The failure mode of the URM façade is separation of the spandrels from two piers due to the weak tensile strength of masonry, followed by independent rocking motion of the piers due to their relatively high height/width ratio.

#### 4.2.2. Nonlinear behaviour of TRM-strengthened façade

The effectiveness of different strengthening schemes and materials on improving the nonlinear performance of the façade is

numerically investigated in this section. The focus is on both the effect of the strengthening material and the strengthening scheme.

**4.2.2.1. Effect of strengthening material.** The strengthening is applied with 5 mm thickness on both sides of the façade. The TRM layers are modelled using the same strategy as presented in Section 3. The mortar mechanical properties are the same as presented in Table 1, and a perfect bond behaviour is assumed at the reinforcement-to-mortar and mortar-to-masonry interfaces. Three types of grids namely: PBO, glass and steel were considered as the reinforcement material, see Table 4 for geometrical and mechanical properties. The PBO and glass fibres are considered as bidirectional and the steel fibres as unidirectional as is the case in most available commercial products. The PBO and glass grids are uniformly applied on the façade. The steel mesh is however applied in horizontal direction in the spandrels and in vertical direction in the piers. The overlapping parts of lintels and piers have thus two orthogonal layers of steel mesh.

The numerical pushover curves for URM and strengthened façade using different types of grids are presented in Fig. 16a. As the results show, the steel-based TRM (presented as RM\_steel) has the highest impact on improving the performance of the façade showing a maximum load factor of 0.63 (142% increasing from URM). This is due to the fact that steel fibres have the largest ten-

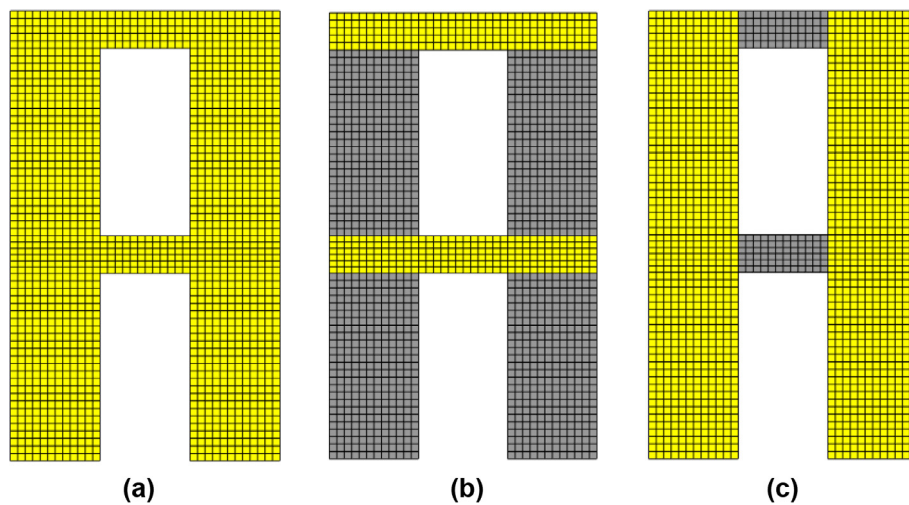


Fig. 17. Strengthening schemes (yellow part means strengthened part, grey part means unstrengthen part): (a) full strengthening scheme; (b) partial strengthening scheme “Steel-H”; (c) partial strengthen scheme “Steel-V”.

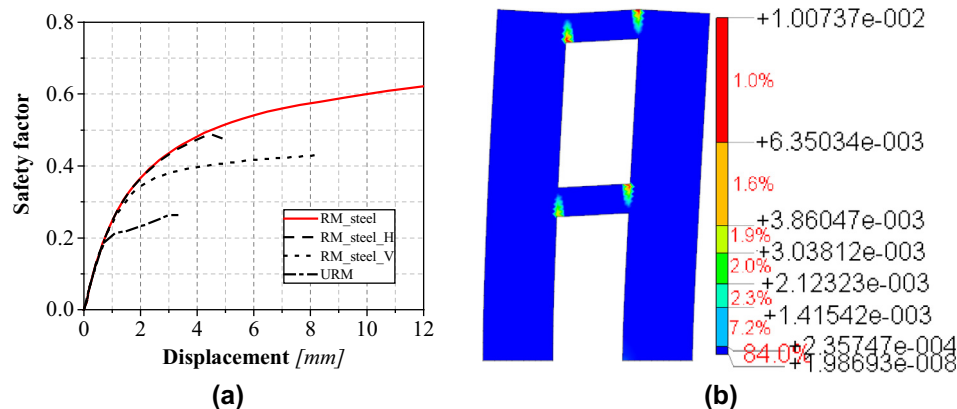


Fig. 18. Pushover analysis results: (a) load–displacement curve of single strengthened façade under different strengthening schemes; (b) principal tensile strains for Steel-V scheme.

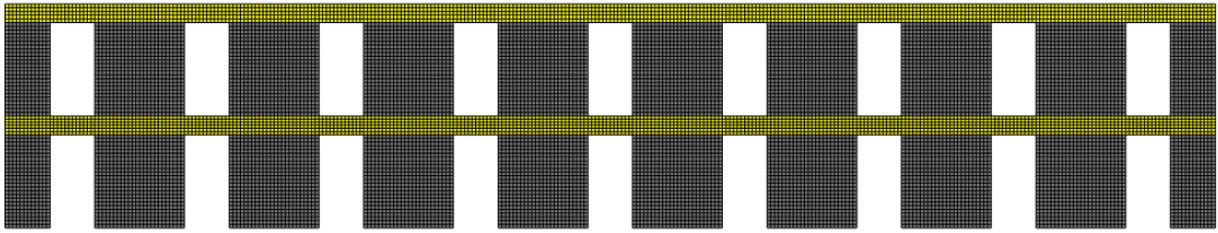


Fig. 19. Strengthening the whole façade with “Steel-H” scheme (yellow part is strengthened, grey part is URM).

sile strength and reinforcement ratio in comparison to other fibres considered in this study. On the other hand, the results show the PBO and glass- strengthened façade have a relatively similar non-linear response with a maximum load factors of 0.45 and 0.40, respectively. Again, it seems that the strengthening does not affect the initial elastic stage of the pushover curves. The failure modes were similar in all the strengthened façades and the results are shown in Fig. 16b for only the RM\_steel façade. Although the failure mode is similar to the URM façade, the strengthening has led to lower strain concentrations at failure points and better distribution of the stresses on the façade.

**4.2.2.2. Effect of strengthening scheme.** Three different strengthening schemes including a complete strengthening application and two different partial strengthening schemes (denoted as “Steel-H” and “Steel-V”) are considered in this section, see Fig. 17.

The pushover curves of the façade strengthened with different schemes are shown in Fig. 18. It can be seen that all strengthening schemes improve the nonlinear behaviour of the structure in terms of capacity and ductility. “RM\_Steel” and “Steel-H” strengthened façades show higher resistance in comparison to “Steel-V”. This can be due to the fact that strengthening of spandrels, not only lead to improving their capacity, but also improves the connection between the piers thus helping in structural integrity. Meanwhile, “Steel-V” strengthening scheme leads to improvement of the piers rocking strength but the spandrels fail due to early cracking, see Fig. 18b. The difference between “RM\_Steel” and “RM\_steel-V” capacity curves shows the importance of strengthening of horizontal spandrels in performance improvement of the structure.

#### 4.3. Behaviour of the whole façade

The whole façade of the Patio da Felicidade building including nine repetitive parts, each one similar to façade No. 22, is simulated and analysed in this section. The strengthening scheme “Steel-H” is used for strengthening of the façade, see Fig. 19. This partial strengthening saves a large amount of material (77% in this case) when compared to application of strengthening to the whole façade, but as observed in the last section it can significantly improve the structure’s lateral performance.

The control point is chosen at the top corner of the façade in the right side. The capacity curves for URM and strengthened façades are presented in Fig. 20. The results show that the strengthened façade has a maximum load factor of 1.1, showing 36% increase from the URM façade ( $\alpha = 0.81$ ). A significant difference can also be observed in the ductility of the structures. The principal strains at the peak load are also presented for URM ( $\alpha = 0.81$ , displacement = 0.62 mm) and strengthened ( $\alpha = 1.1$ , displacement = 1.48 mm) façades in the figure. It can be seen that in the URM façade, the largest cracks are located at the upper corners of top spandrels and at the base. This phenomenon shows the spandrels are weak which leads to separation and independent rocking failure of the piers at the base. As for the strengthened façade, the piers are strongly connected by the strengthened span-

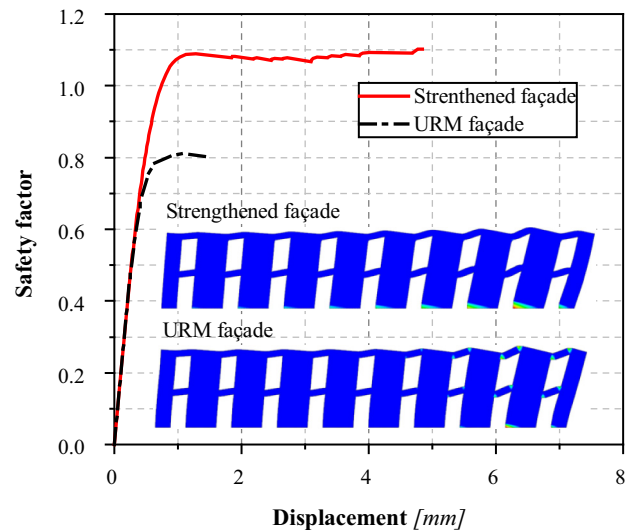


Fig. 20. Pushover curve of URM and strengthened façade.

drels which has resulted in improved lateral performance of the structure.

## 5. Conclusions and recommendations

An extensive numerical investigation was presented aiming at investigation of the nonlinear performance of TRM-strengthened masonry walls. The presented work involved: (1) application of a rational FE macro-modelling approach for simulating the strengthened masonry walls and validation with experimental results; (2) simulating the nonlinear static response (pushover analysis) of TRM-strengthened masonry panels under in-plane loading conditions (i.e. concurrent vertical and lateral loading) and discussion on the effect of different TRM composites on the failure mode and capacity of the panels; (3) investigating the seismic performance of a historical masonry façade (as the case study) in its current condition and after strengthening with TRM composites. In summary, the following conclusions can be drawn:

- A macro-modelling strategy using shell elements with embedded reinforcements was used for simulating the nonlinear response of TRMs. A total strain rotating crack behaviour (smeared crack approach) for the mortar and a linear elastic behaviour until tensile rupture for the fibres was adopted. The modelling strategy showed accurate predictions, in comparison to experimental results, for the non-linear response of TRMs under tensile loads. It was also observed that the JSCE tension softening model is suitable for simulating the post peak response of mortar in TRM composites. There is still a lack of available experimental results on the nonlinear shear response of TRM composites and validation of materials models (or

development of new ones) for such loading conditions remain open. The masonry was also modelled following a macro modelling strategy. The macro modelling strategy was found to be practical in large-scale simulations and to be able to consider all failure mechanisms in these systems with a direct or an indirect manner.

- The FE results showed that TRMs are effective in increasing the in-plane load resistance and ductility of masonry panels. The extent of this increment depends on the vertical load level, boundary conditions and the TRM type used for strengthening. It was also observed that the failure mode can change after strengthening, an important issue that should be considered at the design stage.
- Pushover analysis of the selected case study showed that strengthening of the spandrels with TRM composites can lead to significant improvement of the lateral resistance while saving a large amount of materials when compared to application of TRMs to the whole façade surface. Effectiveness of such a strengthening scheme to improve the out-of-plane performance of masonry components should be investigated in future studies.

## Acknowledgements

The first author is grateful to the SAHC Master Programme for the grant awarded. The second author acknowledges the financial support of the Ministério da Ciência, Tecnologia e Ensino Superior, FCT, Portugal, under the grant SFRH/BPD/92614/2013 as well as the financial support of the European Union's Marie Curie Individual Fellowship program under REA grant agreement No. 701531.

## References

- [1] ElGawady M, Lestuzzi P. A review of conventional seismic retrofitting techniques for URM. In: 13th int brick. p. 1–10.
- [2] Faella C, Martinelli E, Nigro E, Paciello S. Shear capacity of masonry walls externally strengthened by a cement-based composite material: an experimental campaign. *Constr Build Mater* 2010;24(1):84–93.
- [3] Borri A, Castori G, Corradi M. Shear behaviour of masonry panels strengthened by high strength steel cords. *Constr Build Mater* 2011;25(2):494–503.
- [4] Babaeidarabad S, De Caso F, Nanni A. URM walls strengthened with fabric-reinforced cementitious matrix composite subjected to diagonal compression. *J Compos Constr* 2014;18(2):04013045.
- [5] Parisi F, Iovinella I, Balsamo A, Augenti N, Prota A. In-plane behaviour of tuff masonry strengthened with inorganic matrix–grid composites. *Compos Part B Eng* 2013;45(1):1657–66.
- [6] de Felice G, De Santis S, Garmendia L, Ghiassi B, Larrinaga P, Lourenço PB, et al. Mortar-based systems for externally bonded strengthening of masonry. *Mater Struct* 2014;47(12):2021–37.
- [7] De Santis S, de Felice G. Tensile behaviour of mortar-based composites for externally bonded reinforcement systems. *Compos Part B Eng* 2015;68:401–13.
- [8] De Santis S, de Felice G. Steel reinforced grout systems for the strengthening of masonry structures. *Compos Struct* 2015;134:533–48.
- [9] Razavizadeh A, Ghiassi B, Oliveira DV. Bond behaviour of SRG-strengthened masonry units: testing and numerical modelling. *Constr Build Mater* 2014;64:387–97.
- [10] Olivito RS, Codispoti R, Cevallos OA. Bond behaviour of Flax-FRCM and PBO-FRCM composites applied on clay bricks: experimental and theoretical study. *Compos Struct* 2016;146:221–31.
- [11] Bramshuber W, editor. Textile reinforced concrete. State-of-the-art report of RILEM Technical Committee 201-TRC; 2006.
- [12] Ghiassi B, Oliveira DV, Marques V, Soares E, Maljaee H. Multi-level characterization of steel reinforced mortars for strengthening of masonry structures. *Mater Des*. 2016;110:903–13.
- [13] Arboleda D, Carozzi FG, Nanni A, Poggi C. Testing procedures for the uniaxial tensile characterization of fabric-reinforced cementitious matrix composites. *J Compos Constr* 2016;20(3):04015063.
- [14] Carozzi FG, Poggi C. Mechanical properties and debonding strength of Fabric Reinforced Cementitious Matrix (FRCM) systems for masonry strengthening. *Compos Part B Eng* 2015;70:215–30.
- [15] Contamine R, Junes A, Si Larbi A. Tensile and in-plane shear behaviour of textile reinforced concrete: analysis of a new multiscale reinforcement. *Constr Build Mater* 2014;51:405–13.
- [16] Garmendia L, Larrinaga P, García D, Marcos I. Textile-reinforced mortar as strengthening material for masonry arches. *Int J Archit Herit* 2014;8(5):627–48.
- [17] D'Antino T, Carloni C, Sneed LH, Pellegrino C. Matrix–fiber bond behaviour in PBO FRCM composites: a fracture mechanics approach. *Eng Fract Mech* 2014;117:94–111.
- [18] Carozzi FG, Milani G, Poggi C. Mechanical properties and numerical modelling of Fabric Reinforced Cementitious Matrix (FRCM) systems for strengthening of masonry structures. *Compos Struct* 2014;107:711–25.
- [19] Grande E, Imbimbo M, Sacco E. Modelling and numerical analysis of the bond behaviour of masonry elements strengthened with SRP/SRG. *Compos Part B Eng* 2013;55:128–38.
- [20] Papanicolaou C, Triantafillou TC, Lekka M. Externally bonded grids as strengthening and seismic retrofitting materials of masonry panels. *Constr Build Mater* 2011;25(2):504–14.
- [21] Babaeidarabad S, Arboleda D, Loreto G, Nanni A. Shear strengthening of unreinforced concrete masonry walls with fabric-reinforced-cementitious-matrix. *Constr Build Mater* 2014;65:243–53.
- [22] Corradi M, Borri A, Castori G, Sisti R. Shear strengthening of wall panels through jacketing with cement mortar reinforced by GFRP grids. *Compos Part B Eng* 2014;64:33–42.
- [23] Kadam SB, Singh Y, Li B. Strengthening of unreinforced masonry using welded wire mesh and micro-concrete – behaviour under in-plane action. *Constr Build Mater* 2014;54:247–57.
- [24] Gattesco N, Boem I. Experimental and analytical study to evaluate the effectiveness of an in-plane reinforcement for masonry walls using GFRP meshes. *Constr Build Mater* 2015;88:94–104.
- [25] De Santis S, Casadei P, De Canio G, de Felice G, Malena M, Mongelli M, et al. Seismic performance of masonry walls retrofitted with steel reinforced grout. *Earthq Eng Struct Dyn* 2016;45(2):229–51.
- [26] Ismail N, Ingham JM. In-plane and out-of-plane testing of unreinforced masonry walls strengthened using polymer textile reinforced mortar. *Eng Struct* 2016;118:167–77.
- [27] Yardim Y, Lalaj O. Shear strengthening of unreinforced masonry wall with different fiber reinforced mortar jacketing. *Constr Build Mater* 2016;102:149–54.
- [28] Papanicolaou CG, Triantafillou TC, Papathanasiou M, Karlos K. Textile reinforced mortar (TRM) versus FRP as strengthening material of URM walls: out-of-plane cyclic loading. *Mater Struct* 2008;41(1):143–57.
- [29] Harajli M, Elkhatib H, San-Jose JT. Static and cyclic out-of-plane response of masonry walls strengthened using textile-mortar system. *J Mater Civ Eng* 2010;22(11):1171–80.
- [30] Garmendia L, Larrinaga P, San-Mateos R, San-José JT. Strengthening masonry vaults with organic and inorganic composites: an experimental approach. *Mater Des* 2015;85:102–14.
- [31] Borri A, Casadei P, Castori G, Hammond J. Strengthening of brick masonry arches with externally bonded steel reinforced composites. *J Compos Constr* 2009;13(6):468–75.
- [32] Larrinaga P, Chastre C, Biscaia HC, San-José JT. Experimental and numerical modelling of basalt textile reinforced mortar behaviour under uniaxial tensile stress. *Mater Des* 2014;55:66–74.
- [33] Bertolesi E, Carozzi FG, Milani G, Poggi C. Numerical modelling of Fabric Reinforced Cementitious Matrix composites (FRCM) in tension. *Constr Build Mater* 2014;70:531–48.
- [34] Basili M, Marcari G, Vestroni F. Nonlinear analysis of masonry panels strengthened with textile reinforced mortar. *Eng Struct* 2016;113:245–58.
- [35] Bertolesi E, Milani G, Poggi C. Simple homonomic homogenization model for the non-linear static analysis of in-plane loaded masonry walls strengthened with FRCM composites. *Compos Struct* 2016;158:291–307.
- [36] Garofano A, Ceroni F, Pecce M. Modelling of the in-plane behaviour of masonry walls strengthened with polymeric grids embedded in cementitious mortar layers. *Compos Part B Eng* 2016;85:243–58.
- [37] Holler S, Butenweg C, Noh SY, Meskouris K. Computational model of textile-reinforced concrete structures. *Comput Struct* 2004;82(23–26):1971–9.
- [38] Graf W, Hoffmann A, Möller B, Sickert JU, Steinigen F. Analysis of textile-reinforced concrete structures under consideration of non-traditional uncertainty models. *Eng Struct* 2007;29(12):3420–31.
- [39] Lourenço PB, Rots JG, Blaauwendraad J. Continuum model for masonry: parameter estimation and validation. *J Struct Eng ASCE* 1998;146(6):642–52.
- [40] DIANA. Displacement analysis finite element software. V. 9.6, TNO Building Division, 2015, Delft, The Netherlands.
- [41] Japanese Society of Civil Engineering (JSCE). Guidelines for Concrete No. 15: Standard Specifications for Concrete Structures – Design. 2010.
- [42] Bieniawski ZT, Hawkes I. Suggested methods for determining tensile strength of rock materials. *Int J Rock Mech Min Sci* 1978;15(3):99–103.
- [43] Ghiassi B, Lourenço PB, Oliveira DV. Effect of environmental aging on the numerical response of FRP-strengthened masonry walls. *J Struct Eng* 2016;142(1):4015087.
- [44] Grande E, Milani G, Sacco E. Modelling and analysis of FRP-strengthened masonry panels. *Eng Struct* 2008;30(7):1842–60.
- [45] Grande E, Imbimbo M, Sacco E. Finite element analysis of masonry panels strengthened with FRPs. *Compos Part B Eng* 2013;45(1):1296–309.
- [46] Fat K. A study of masonry structures of Macau. Report; 2012.
- [47] Richter M, Zastrau BW. On the nonlinear elastic properties of textile reinforced concrete under tensile loading including damage and cracking. *Mater Sci Eng, A* 2006;422(1–2):278–84.